ISSN 1 746-7233, England, UK
World Journal of Modelling and Simulation
Vol. 6 (2010) No. 3, pp. 198-204

A modelling and simulation approach of electromagnetic field in organic photovoltaic devices

M. R. Merad Boudia[1] , A. Cheknane[2*]

[1] Unit of Research Materials & Renewable Energies, University Abou baker Belkaid of Tlemcen, Tlemcem 13000, Algeria

[2] Laboratory of Valorization of Renewable Energies and Aggressive Environments, University Amar Telidji of Laghouat, Laghouat 03000, Algeria

(*Received 20 September 2009, Revised 25 March 2009, Accepted 27 May 2010*)

Abstract. Of the many properties of materials, the optical properties are undoubtedly among the most useful and interesting, specially for inorganic and organic semiconductors. In this paper, we report our results on the electrical and optical modelling of a mono or multi-layer organic photovoltaic device, in which the incident light of sun is absorbed in the active layer. The influence of the optical parameters and thicknesses of different layers had been taken into account to improve the device performance. A composite of poly (2-methoxy-5-(39,79-dimethyloctyloxy)-1,4-phenylene-vinylene) (MDMO-PPV) and (6,6)-phenyl-C61-butyric acid methyl ester (PCBM) is used as photo-active material, sandwiched between a transparent Indium Tin Oxide (ITO)-electrode and an Al backside contact. This study aims to show essentially the optical effects of an extra interfacial layer of poly (3, 4-ethylenedioxythiophene)/(poly(styrenesulfonate) (PEDOT/PSS) on top of the ITO-electrode. Our objective is to present a combination of two matrix-based method which makes it possible the description of electric and magnetic fields according to the total impedance of the system. The essential result of this work is the minimization of losses in the generation rate of charge carriers for an organic solar cell, produced by the insertion of a protective layer. In addition the reflectivity versus the active layer thickness and the angle of incidence has been discussed.

Keywords: organic solar cells, electro-optical modelling, generation rate, refractive index

1 Introduction

In these last years several research was undertaken on the study of the interaction between the incident light with the photovoltaic devices of organic semiconductors. The modelling of optical absorption in organic solar cells has a great importance in the prediction of the electro-optical properties of these devices because the dissociation of charges is assisted strongly by the application of an electric field in organic materials.

[7] have presented a method of optimization of the electromagnetic field in the organic solar cells, and an electro-optical modelling of these cells describing the generation rate of excitons based on the calculation of the profile of absorbed energy. V. V. Fillippov and L. M. Serebryakova presented in [2] a concrete analysis of interference effects on the spatial field distribution. Another research group[8, 9] made the minimization of the optical losses in the bulk heterojunction solar cells by using the complex index of refraction and ellipsometry.

The electromagnetic properties of reflection, transmission and absorption have an importance in the optical characterization of multi-layer system used in inorganic and organic photovoltaic devices. They describe the interaction of the incident light with the various layers of the system. Depending on the optical constants and the thicknesses of mono-layers we use here a matrix transmission[5] to calculate the electromagnetic field for all the device structures.

* *E-mail address*: a.cheknane@mail.lagh-univ.dz.

The basic idea, in this paper, is to use a simple matrix 2×2 to describe the propagation of an electromagnetic field of a section to another of the device. For each discrete section there is a single matrix 2×2. The electric and the magnetic fields were related by a second matrix[10] containing the thickness of the active layer. We beginning our study by denoting some definitions of the interaction radiation-matter between a propagated wave and double, multi-layered structures, then we present our model of simulation basing on matrix formalism. Finally, we apply this model to a certain BHJ solar cells and we discuss the results of our study.

2 Theory

In this section we present a part of fundamental mechanisms of matter-radiation interaction, being given a solid body crossed by a sinusoidal monodirectionnal wave being propagated on OZ axis, we have two cases to consider:

2.1 Case of a double-layered system

When the light travels of the first medium with n_1 index of refraction in the second medium with n_2 index of refraction, the amplitudes of the electric field of the electromagnetic wave reflected and transmitted of the interface are governed by the coefficients of Fresnel[6] (Fig. 1):

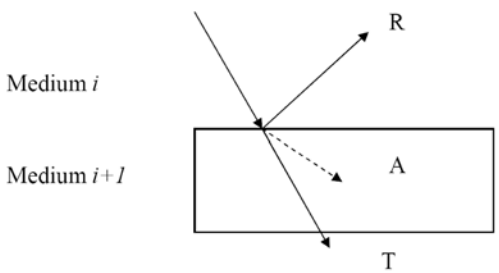

Fig. 1. Electrodynamic multi-layer system

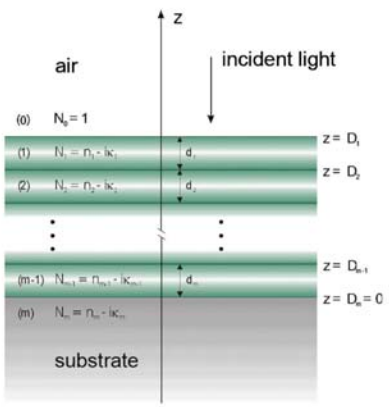

Fig. 2. Electrodynamic multi-layer system

where A, R and T are the absorptance, the reflectance and the transmittance of the medium.

The Fresnels coefficients are defined as being the relationship between the amplitudes of the electric field before and after an interface. In the case of a system of two mediums i and $i+1$, the reflection of a beam with normal incidence on the interface gives the coefficient of Fresnel: $r = E_e/E_i$, where E_e and E_i are the electric fields after and before an interface respectively.

For linear, isotropic and homogeneous mediums, we can calculate the coefficients of Fresnel directly with the indices of refraction. If the angle of incidence of the beam on the medium is null, we have [6]:

$$r_{TE} = \frac{n_1 - n_2}{n_1 + n_2}, \qquad t_{TE} = \frac{2 * n_1}{n_1 + n_2}, \qquad r_{TM} = \frac{n_2 - n_1}{n_1 + n_2}, \qquad t_{TM} = \frac{2 * n_1}{n_1 + n_2}$$

2.2 Case of a multi-layer system

Two methods of calculation are possible:

A method where we wrote incident, reflected and transmitted fields, layer by layer, and we note that the boundary conditions of these fields must be satisfied[3].

Fig. 2 illustrates an electrodynamic multi-layer system. Considering a perpendicular incidence of light to against direction 'Z'. In the classical model in any interface between two layer, the incident light is divided into a transmitted part and a reflected part. In l, $l+1$ the reflected parts fall behind to $l-1$, l, where they are divided still in transmitted and reflected parts. Consequently it comes to the multiple reflections in each layer.

Based on Maxwell's equations and conditions of continuity, we obtain the partial waves for the multi-layer system:

The incident wave: $\overrightarrow{E}^e(\overrightarrow{r}) = \overrightarrow{A}^e e^{-i\overrightarrow{K}^e\overrightarrow{r}}$;

The reflected wave: $\overrightarrow{E}^r(\overrightarrow{r}) = \overrightarrow{A}^r e^{-i\overrightarrow{K}^r\overrightarrow{r}}$;

The wave $l-$ (against direction of Z): $\overrightarrow{E}^{l-}(\overrightarrow{r}) = \overrightarrow{A}^{l-} e^{-i\overrightarrow{K}^{l-}\overrightarrow{r}}$;

The wave $l+$ (against direction of Z): $\overrightarrow{E}^{l+}(\overrightarrow{r}) = \overrightarrow{A}^{l+} e^{-i\overrightarrow{K}^{l+}\overrightarrow{r}}$;

The transmitted wave: $\overrightarrow{E}^t(\overrightarrow{r}) = \overrightarrow{A}^t e^{-i\overrightarrow{K}^t\overrightarrow{r}}$;

$(l = 0, 1, 2, 3, \cdots, m-1)$.

With the wave vector, the amplitude vector and by the use of the coefficients of Fresnel we can calculate the electric field of the incident, reflected and transmitted wave, as well as for the components of the waves in the various layers.

The incidental wave: $E_x^e(z) = e^{-i(k_x^e x + k_x^e z)} A_x^e$;

The reflected wave: $E_x^e(z) = -r_{om} e^{-2ik_z^e D_1} e^{-i(k_x^e x - k_x^e z)} A_x^e$;

The wave $l-$: $E_x^{l-}(z) = \frac{k_z^l}{k_z^e}\frac{t_{om}}{t_{lm}} e^{ik_z^l D_{l+1}} e^{-ik_z^e D_1} e^{-i(k_x^e x - k_x^e z)} A_x^e$;

The wave $l+$: $E_x^{l+}(z) = -\frac{k_z^l}{k_z^e}\frac{t_{om}}{t_{lm}} r_{lm} e^{-ik_z^l D_{l+1}} e^{-ik_z^e D_1} A_x^e e^{-i(k_x^e x - k_x^e z)} A_x^e$;

The transmitted wave: $E_x^t(z) = \frac{k_z^t}{k_z^e} t_{om} e^{-ik_z^t D_m} e^{-ik_z^e D_1} e^{-i(k_x^e x - k_x^t z)} A_x^e$.

A matrix method which we describe after here:

The multiplication of the matrices[8] will describe how the wave propagates by the whole device. Fig. 3 shows the arrangement of propagation of the forwards and towards fields in the back of the device. The Eq. (1) gives

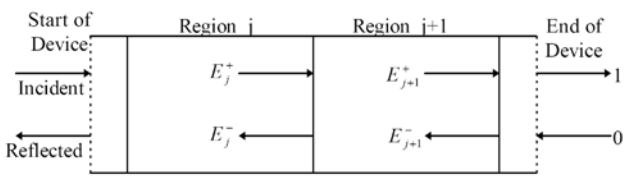

Fig. 3. Arrangement of fields' propagation the forwards and the back of the device

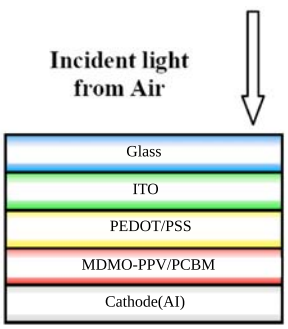

Fig. 4. Diagram of an organic solar cell

the electric field in $(j+1)^{th}$ layer, or the 1^{st} term is the component of the transmitted wave in the layer $(j+1)$, and the 2^{nd} term of the reflected wave.

$$\begin{bmatrix} E_{j+1}^+ \\ E_{j+1}^- \end{bmatrix} = \varphi \begin{bmatrix} E_j^+ \\ E_j^- \end{bmatrix}, \tag{1}$$

where the matrix φ is a function of layers thicknesses and Fresnel's coefficients.

Since optical energy is a measurable quantity, the first stage in the calculation of the optical generation rate is to calculate the Poynting vector brought back to an average per hour:

$$\langle P_j \rangle = \frac{1}{2}[E_j \times H_j^*]. \tag{2}$$

The negative derivation of Poynting vector is a measurement of the absorbed energy for each position of the active layer. Let us divide this quantity by the photon energy we obtain the photon generation rate. Finally

the summation of this quantity on the entire visible spectrum (on the wavelength rang: $350\ nm - 900\ nm$) gives the optical generation rate:

$$G_{\text{Optic}}(x) = \sum_{h\nu_{optic}} G_{\text{v,Optic}}(x). \tag{3}$$

The relations managing electric and magnetic fields and which allow the direct passage of a wave from a layer to the other are given by:

$$\begin{vmatrix} E_{j-1} \\ H_{j-1} \end{vmatrix} = |\psi| \begin{vmatrix} E_j \\ H_j \end{vmatrix}, \tag{4}$$

where ψ_m is a 2×2 matrix which contains the permittivity values for each medium.
According to the last matrix we can also calculate the reflectivity R of our multilayer device and we compare this parameter with that published by [4]:

$$R = \frac{I_{\text{Glass-ITO}} - I_0(1 - R_{\text{Air-Glass}})e^{-ah}}{I_{\text{Glass-ITO}} R_{\text{Air-Glass}} r^{-2\alpha h}}, \tag{5}$$

with I_0 is the incidence irradiance; $I_{\text{Glass-ITO}}$ is the light intensity in the glass; $R_{\text{Air-Glass}}$ is the reflectivity of the air-glass interface; α is the absorption coefficient of the glass; h is the thickness of the glass.

3 Application

We can apply the model described previously to an organic solar cell of Glass/ITO/(PEDOT-PSS)/(MDMO PPV/PCBM)/Al composition manufactured by [1]. The thickness of ITO anode is supposed $d = 140\ nm$, layer PEDOT/PSS with also a thickness of $140\ nm$, the counter electrode in Aluminium has generally a thickness of $30\ nm$, this last material is supposed to be completely reflective in our simulations, with the various thicknesses of the active layer.

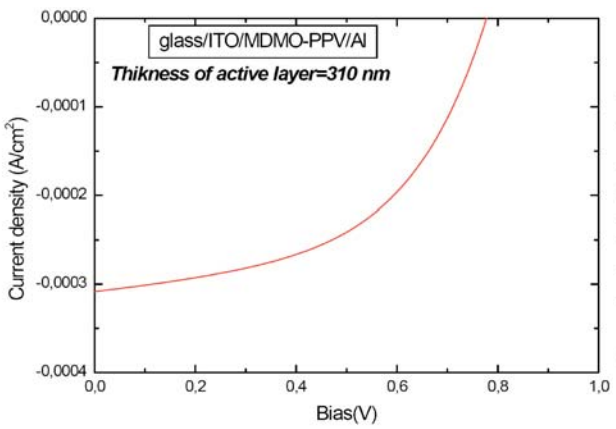

Fig. 5. J-V characteristic of a manufactured organic solar cell[3]

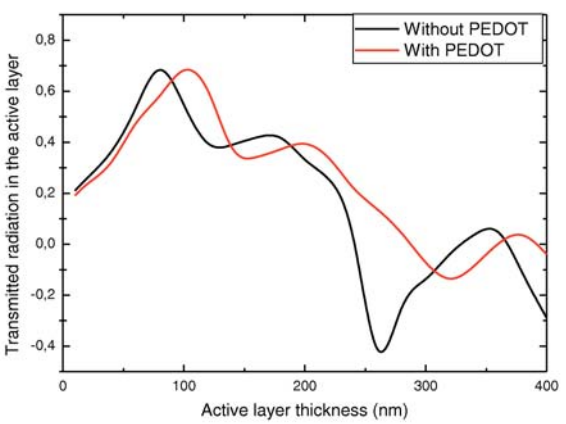

Fig. 6. Energy transmitted in the active layer of an organic solar cell with and without additional layer in PEDOT/PSS

A J-V characteristic of one of prototypes that we use has a thickness of $310\ nm$ of the active layer is shown in Fig. 5. This prototype is used also by [3].

4 Results and discussion

In this section we discuss the dependence on the thickness of the electric field, the generation rate and the reflectivity of the device described previously.

Fig. 6 illustrates the profile of the electric field in each layer of the photovoltaic device according to the thickness of the active layer. The digital simulation shows that the protective coating in PEDOT/PSS affects clearly the luminous energy transmitted in the active layer when this energy is decreased for very thinner active layers because there is a big region of reflections at the counter electrode in A1. Figs. 7, 8 and 9 give

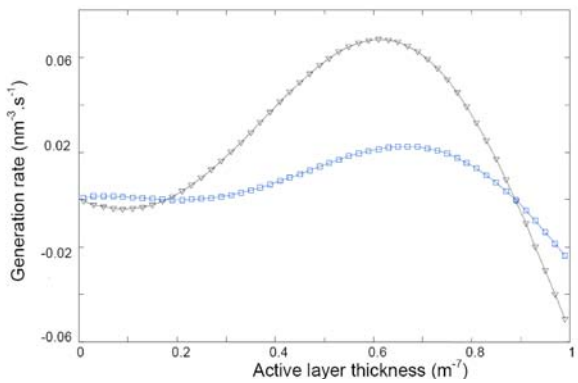

Fig. 7. Generation rate in the active layer of an organic solar cell without additional layer for thicknesses of 100 nm

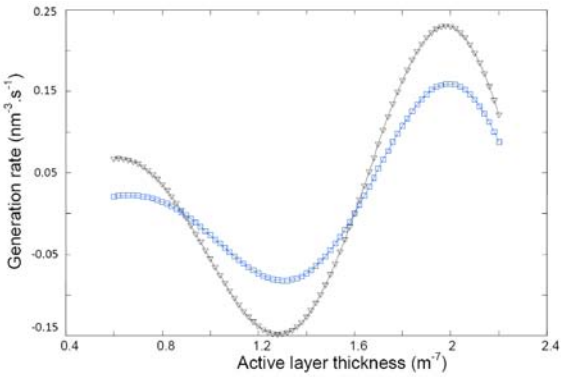

Fig. 8. Generation rate in the active layer of an organic solar cell without additional layer for thicknesses of 220 nm

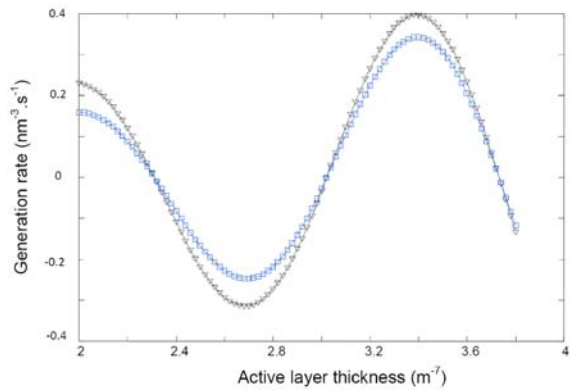

Fig. 9. Generation rate in the active layer of an organic solar cell without additional layer for thicknesses of 350 nm

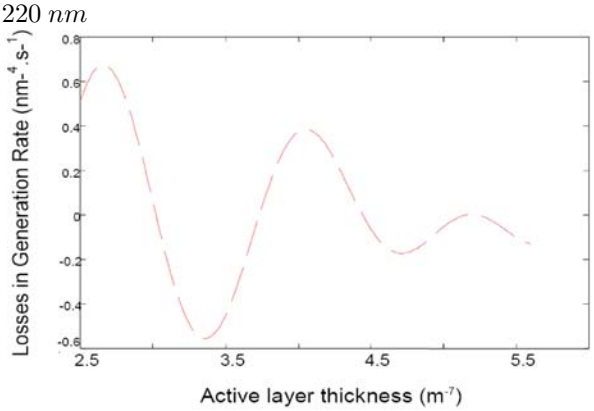

Fig. 10. Losses in generation rate for thicknesses more than 250 nm

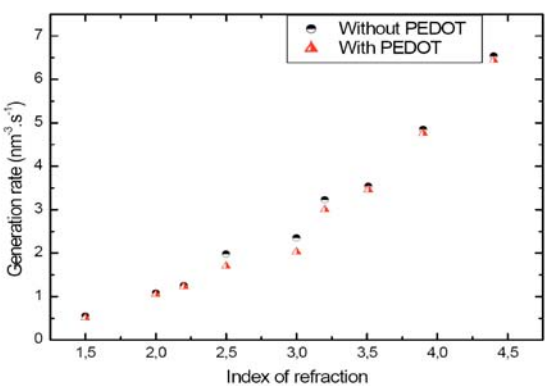

Fig. 11. Generation rate versus refraction index of in an organic solar cell

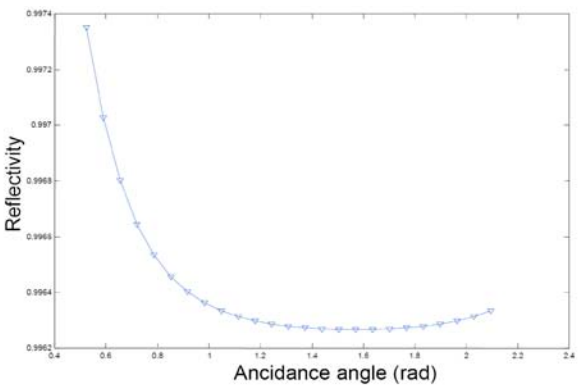

Fig. 12. Reflectivity of the device versus the angle of incidence

the generation rate of carriers in an organic solar cell containing active material in MDMO-PPV/PCBM with

additional layer (square lines) and without (triangle lines) in PEDOT/PSS according to the thickness of the active layers 100 nm, 220 nm and 350 nm. It is clear that the losses in the generation rate Fig. 10 produced by the protective layer decrease when the thickness of the active layer is increased and it converge to zero when we extrapolate our simulations at 650 nm. The generation rate is affected by the PEDOT/PSS layer versus the index of refraction as it is shown in Fig. 11.

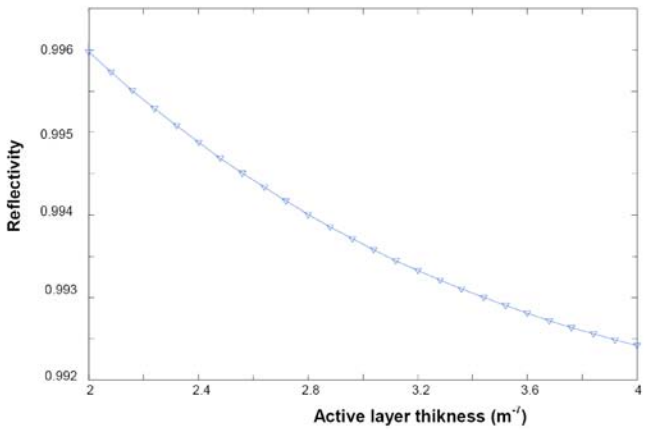

Fig. 13. Reflectivity of the device versus the active layer thickness. Solid line (global impedance of the system). Triangles (model published by H. Hoppe et al.[4])

Fig. 12 illustrates the dependence on the angle of incidence for the reflectivity of the device system detailed in Fig. 4, this parameter is minimized on the $(5\pi/12 - 7\pi/12)$ radian range at 400 nm of thickness of the active layer. Reflectivity is calculated from the effective impedance of entry of the device and compared with that published by H. Hoppe et al. (Fig. 13), so it is clear that it is in good agreement with this model.

5 Conclusion

In summary, the performances of organic solar cells devices with PEDOT-PSS as protective layer were investigated and compared trough an optical modelling. We presented in this paper the results of modelling and digital simulation which describe the evolution of the magnetic and electric fields in bulk heterojunction solar cells, as well as the optimization of the generation rate of charge carriers that depends essentially on the electric field distribution, according to the thickness of the active layer and the index of refraction. The study of the reflectivity of the photovoltaic device versus the angle of incidence and the thickness of the active layer are detailed in the end of this work. Our results of simulation are in good agreement with those published in the literature by the combination of two recent methods; the first is applied in inorganic devices and the second is applied in optical telecommunications. In our work we applied these two recent methods to enhance the performance of photovoltaic devices. In our future work we plan to re-study the existing cell. For each structure we would add a buffer layer at the mettalic cathode. This structure will increase absorption of light of every given area of the light spectrum and optimization of this type of solar cells is our future perspective.

References

[1] T. Aernouts, W. Geens, et al. Extraction of bulk and contact components of the series resistances in organic bulk donor-acceptor-heterojunctions. *Thin Solid Films*, 2002, **403-404**: 297–301.

[2] V. Filppov, L. Serebryakova. Optical characteristics of a multilayer photovoltaic cell for oblique incidence of light. *Journal of Applied Spectroscopy*, 2007, **74**(6).

[3] D. Gruber, G. Meinhardt, W. Papousek. Modelling the light absorption in organic photovoltaic devices. *Solar Energy Materials and Solar Cells*, 2004.

[4] H. Hoppe, N. Arnold, et al. Modeling the optical absorption within conjugated polymer/fullerene-based bulk-heterojunction organic solar cells. *Solar Energy Materials and Solar Cells*, 2003, **80**: 105–113.

[5] B. Kim, E. Garmire. Comparison between the Matrix Method and the Coupled-Wave Method in the Analysis of Bragg Reflector Structures. *Journal of the Optical Society of America A*, 1992, **9**: 132–136.

[6] L. Li. The design of Optical Thin Film Coatings with total and total Frustrated internal Reflection with Total and total Frustrated internal reflection. *Optics & Photonics News*, 203.

[7] F. Monestier, J. Simon, et al. Modeling the short-circuit current density of polymer solar cells based one p3ht:pcbm blend. *Solar Energy Materials and Solar Cells*, 2007, 405–410.

[8] A. Moulé, K. Meerholz. Interference method for the refractive determination of the complex index of thin polymer layers. *Applied Physics Letters*, 2007, **91**(6): 061901.

[9] A. Moul, K. Meerholz. Minimizing optical losses in bulk heterojunction polymer solar cells applied. *Physics*, 2007, 721–727.

[10] A. Priou. Bianisotropic and Bi- isotropic Media and Applications. *Progress in Electromagnetic Research*, 1994, **9**. EMW Publishing.

Using model system (2), we obtain

$$\frac{\beta\eta AS}{NI} = \frac{I'}{I} - \frac{\beta S}{N} + (\mu + \kappa), \tag{30}$$

$$\frac{\kappa I}{A} = \frac{A'}{A} + (\mu + \delta). \tag{31}$$

Substituting (30) and (31) into (28) and (29) respectively gives

$$g_1 = \frac{I'}{I} - \mu - \frac{\beta(I + \eta A)}{N} - \frac{\beta AS(I + \eta A)}{N^2 I}, \tag{32}$$

$$g_2 = \frac{I'}{I} - \mu. \tag{33}$$

Therefore, $\sup\{g_1(t), g_2(t)\} \leq \frac{I'}{I} - \mu$ and

$$\int_0^\omega \sup\{g_1(t), g_2(t)\}\mathrm{d}t \leq \log I(t)|_0^\omega - \mu\omega = -\mu\omega < 0.$$

This relationship and (27) imply that $V(t) \to 0$ as $t \to \infty$ and in turn that $(X(t), Y(t), Z(t)) \to 0$ as $t \to \infty$ by (22). As a result, the second compound system (19) is asymptotically stable and the periodic solution $(S(t), I(t), A(t))$ is asymptotically stable by Theorem 6.

Theorem 7. *If $\mathcal{R}_0 > 1$, then the unique endemic equilibrium $\mathcal{E}_e$ is globally asymptotically stable for model system (2) in $\overset{\circ}{\Phi}$.*

Proof. From the condition (1) of Theorem 5, uniformly persistent property of the solution of model system (2) can be concluded[3]. Let $B = \mathcal{E}_0$, Theorem 1 implies that, when $\mathcal{R}_0 > 1$, B^s is just contained in the $S-$axis and thus just in the boundary of Φ. It also implies that B^s is isolated in Φ. When $\mathcal{R}_0 > 1$, model system (2) satisfies the conditions of Theorem 4 of [10], namely, (i) the maximal compact invariant set B in the boundary of Φ is isolated and (ii) the stable set B^s of B is contained in the boundary of Φ. Therefore, model system (2) is uniformly persistent in Φ when $\mathcal{R}_0 > 1$. By looking at the Jacobian matrix of model system (2) and choosing matrix $\boldsymbol{H}$ as $\boldsymbol{H} = \mathrm{diag}(1, -1, 1)$, we can see that $\boldsymbol{HJ}(S, I, A)\boldsymbol{H}$ has non positive of-diagonal elements for all $(S, I, A) \in \Phi$. Thus we can verify that model system (2) is competitive with respect to the partial ordering defined by the orthant $\Phi = \{(S, I, A) \in \mathbb{R}^3 : S \geq 0, I \geq 0, A \geq 0\}$ [23]. From [9, 16, 23], we note that model system (2) satisfies Poincarè-Bendixson property. By Lemma 3 and Theorem 3, we note that model system (2) is satisfied with every condition of Theorem 5, so the unique endemic equilibrium of model system (2) is globally asymptotically stable.

3 Numerical simulations

In order to illustrate some of the analytical results in this study, numerical simulations of model system (2) are carried out using a set of parameter values given in Tab. 3. We use Matlab software for the numerical simulations.

Figs. 3 (a) and 3 (b) illustrate the phase plane portraits of (a) SI-plane, (b) SA-plane for $\mathcal{R}_0 = 0.341 < 1$ $(p = 0.011)$ showing convergence to the disease free equilibrium in line with Lemma 1. Similarly, Figs. 3 (a) and 3 (b) illustrate the phase plane portraits of (a) SI-plane, (b) SA-plane for $\mathcal{R}_0 = 3.41 > 1$ $(p = 0.11)$ showing convergence to the endemic equilibrium in line with Theorem 3.

4 Summary and concluding remarks

In this study an HIV/AIDS epidemic model incorporating constant recruitment and sexually active AIDS individuals is presented and analysed. Using a Lyapunov function and LaSalle's invariant set theorem, we proved the global asymptotic stability of the disease-free equilibrium. Local asymptotic stability of the endemic equilibrium is derived using the center manifold theory and Poincarè-Bendixson property is used to prove its global asymptotic stability. The analytical and numerical findings suggest that the disease dies out (or is controlled) when $\mathcal{R}_0 < 1$ or persists in a population with endemicity when $\mathcal{R}_0 > 1$.

Table 1. Data for the HIV/AIDS model

Parameter	Symbol	Value	Source
Recruitment rate	Λ	29 yr^{-1}	Estimate
Rate of acquiring new sexual partners	c	3 partners/year	[17]
Probability of transmission	p	0.011-0.95	[17]
Rate of progression to AIDS	κ	0.125 yr^{-1}	[17, 18]
Natural death rate	μ	0.02 yr^{-1}	[17, 18]
AIDS-related death rate	δ	0.333 yr^{-1}	[17, 18]
Enhancement factor	η	1.4	[18]

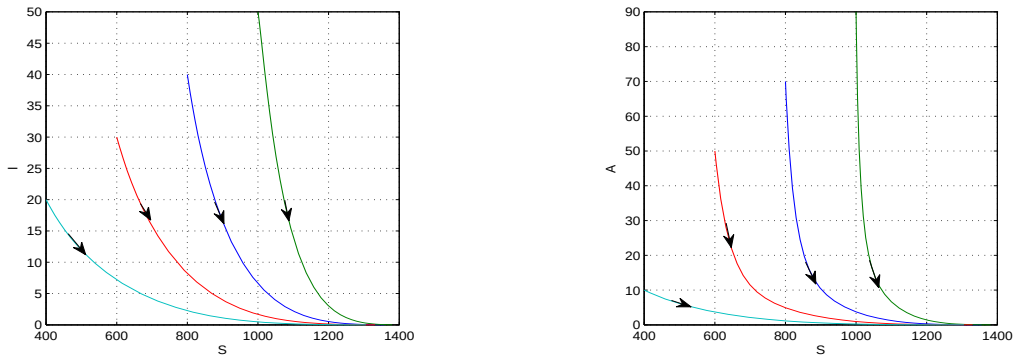

(a) (b)

Fig. 2. Phase plane portraits of (a) SI-plane, (b) SA-plane for $\mathcal{R}_0 = 0.341 < 1$ ($p = 0.011$) showing convergence to the disease free equilibrium using parameter values in Tab. 3 and varying initial conditions

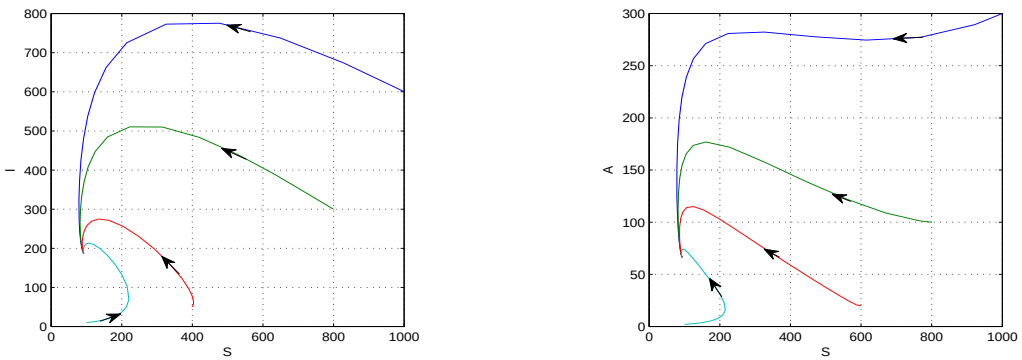

(a) (b)

Fig. 3. Phase plane portraits of (a) SI-plane, (b) SA-plane for $\mathcal{R}_0 = 3.41 > 1$ ($p = 0.11$) showing convergence to the endemic equilibrium using parameter values in Tab. 3 and varying initial conditions

References

[1] R. Anderson, R. May. *Infectious diseases of humans*. Oxford Univesity Press, London/New York, 1991.

[2] F. Brauer, C. Castillo-Chavez. Mathematical models in population biology and epidemiology. **in:** *221 Texts in Applied Mathematics Series*, 40, Springer-Verlag, New York, 2001.

[3] G. Butler, P. Waltman. Persistence in dynamical systems. **in:** *Proceedings of the American Mathematical Society*, *223*, vol. 96, 1986, 425–430.

[4] J. Carr. *Applications of Centre Manifold Theory*. Springer-Verlag, New York, 1981.

[5] C. Castillo-Chavez, Z. Feng, W. Huang. On the computation of r_0 and its role on global stability. 2002. (math.la.-asu.edu/chavez/2002/JB276.pdf).

[6] C. Castillo-Chavez, B. Song. Dynamical models of tuberculosis and their applications. *Mathematical Biosciences and Engineering 228*, 2004, **1**(2): 361–404.

[7] O. Diekmann, H. J, J. Metz. On the definition and computation of the basic 230 reproduction ratio r0 in models for infectious diseases in heterogeneous populations. *Journal of Mathematical Biology*, 1990, **231**: 365–382.

[8] H. Hethcote. The mathematics of infectious diseases. *SIAM Review*, 2000, **42**(4): 599–653.
[9] M. Hirsch. Systems of differential equations which are competitive or cooperative, IV: Structural 234 stabilities in three dimensional systems. *SIAM Journal on Mathematical Analysis*, 1990, **21**: 1225–1234.
[10] J. Hofbauer, J. So. Uniform persistence and repellors for maps. **in:** *Proceedings of the American Mathematical Society*, *236*, vol. 107, 1989, 1137–1142.
[11] A. Lansky, A. Nakashima, J. Jones. Risk behaviors related to heterosexual transmission from HIV2 38 infected persons. *Sex Transm Dis*, 2000, **27**: 483–489.
[12] J. LaSalle. *The Stability of Dynamical Systems, CBMS-NSF Regional Conference Series in Applied 240 Mathematics*, vol. 25. SIAM: Philadelphia, 1976.
[13] M. Li, J. Graef, et al. Global dynamics of a seir model with a varying total 242 population size. *Mathematical Biosciences*, 1999, **160**: 191–213.
[14] M. Li, J. Muldowney. A geometric approach to the global-stability problems. *SIAM Journal on Mathematical Analysis*, 1996, **27**: 1070–1083.
[15] M. Li, J. Muldowney. Global stability for the SEIR model in epidemiology. *Mathematical Biosciences*, 1995, **125**(244): 155–164.
[16] M. Li, L. Wang. Global stability in some SEIR epidemic models. *Institute of Management Accountants*, 2002, **126**: 295–311.
[17] Z. Mukandavire, W. Garira, C. Chiyaka. Asymptotic properties of an hiv/aids model with a time 249 delay. *Journal of Mathematical Analysis and Applications*, 2007, **330**(2): 916–933.
[18] Z. Mukandavire, A. Gumel, et al. Mathematical Analysis of a Model for 251 HIV-Malaria Co-infection. *Mathematical Biosciences and Engineering*, 2009, **6**(2): 333–363.
[19] J. Muldowney. Compound matrices and ordinary differential equations. *Rocky Mountain Journal of Mathematics*, 1990, **20**(253): 857–872.
[20] A. Nicolosi, M. Musicco, et al. Risk factors for woman-to-man sexual transmission 255 of the human immunodeficiency virus. *Journal of Acquired Immune Deficiency Syndromes*, 1994, **7**: 296–300.
[21] T. OBrien, M. Busch, et al. Heterosexual transmission of human 257 immunodeficiency virus type 1 from transfusion recipients to their sex partners. *Journal of Acquired Immune Deficiency Syndromes*, 1994, **7**: 705–710.
[22] L. Perko. Differential Equations and Dynamical Systems. **in:** *Text in Applied Mathematics*, *260*, vol. 7, Springer, Berlin, 2000.
[23] H. Smith. Systems of ordinary differential equations which generate an order preserving flow. *SIAM Review*, 1988, **30**: 87–113.
[24] UNAIDS. *Report on the Global AIDS Epidemic*. Geneva, 2006.
[25] UNAIDS/WHO. *AIDS epidemic update*. Geneva, 2005.
[26] P. van den Driessche, J. Watmough. Reproduction numbers and sub-threshold endemic equilibria 264 for compartmental models of disease transmission. *Mathematical Biosciences*, 2002, 29–48.